POLITECNICO DI TORINO
Repository ISTITUZIONALE

Comparison of depth-averaged and full-3D model for the benchmarking exercise on landslide runout

Original
Comparison of depth-averaged and full-3D model for the benchmarking exercise on landslide runout / Pirulli, M., Leonardi, A., Scavia, C.. - ELETTRONICO. - (2018), pp. 240-253. (Proceedings of the 2nd JTC1 worshop on Triggering and Propagation of Rapid Flow-like Landslides, Hong Kong (China) 3-5 December 2018).

Availability:
This version is available at: 11583/2972086 since: 2022-10-05T10:16:23Z

Publisher:
ISSMGE

Published
DOI:

Terms of use:

This article is made available under terms and conditions as specified in the corresponding bibliographic description in the repository

Publisher copyright

(Article begins on next page)

19 November 2026

Comparison of depth-averaged and full-3D model for the benchmarking exercise on lanslide runout

M. Pirulli, A. Leonardi & C. Scavia
Politecnico di Torino
Department of Structural, Geotechnical and Building Engineering
Corso Duca degli Abruzzi 24, 10129, Turin, Italy

ABSTRACT

Two models, with fundamental differences in their approaches, are used for modeling benchmarking exercise. The first, RASH^{3D}, is based on a set of depth-averaged equation, solved in an Eulerian framework. The second, HYBIRD, employs a 3D Lattice-Boltzmann Model (LBM), i.e. the conservation equations are not depth-averaged and therefore multiple velocity measures are available over the depth. The model output are compared for what concerns the Yu-Tung debris flow back-analysis. Two additional cases are then analyzed using RASH^{3D}.

1 INTRODUCTION

Landslide-related phenomena, including debris flows, mudflows and rock avalanches, are one of the major sources of concern for infrastructure and communities located on mountainous terrain. Notwithstanding the efforts devoted on understanding and mitigating these hazards, the related casualties keep growing worldwide, and in particular in developing countries. This is probably due to a combination of environmental changes and of the rise of urbanization in formerly sparsely populated areas (Froude & Petley, 2018). Predicting the evolution of these phenomena with the use of numerical modeling is of vital importance. Information on the material velocity during an event, its run-out distance, and the final shape of the deposit, can all allow to develop more precise hazard maps, and design more effective countermeasure.

For the Second JTC1 Workshop - Triggering and Propagation of Rapid Flow-like Landslides, the group at Politecnico di Torino agreed to benchmark its current modeling capabilities. Two methods, both implemented in in-house codes, are therefore tested in this work. The methods are different on various theoretical and practical aspects. The first method, implemented in the code RASH^{3D} (Pirulli, 2005, Pirulli et al., 2007), solves a set of depth-averaged versions of the Navier-Stokes equations. The second, implemented in the code HYBIRD (Leonardi et al., 2016), is based on the Lattice-Boltzmann Method (LBM) and, rather than solving the Navier-Stokes equation directly, performs a solution of the Boltzmann equation. More details about the numerical methods are given in the next sections. However, a key difference in the two approaches is already remarked here. RASH^{3D} follows a standard depth-averaging technique, where the topography is implemented using (x,y,z) points, but only a single value for depth-averaged quantities (height, velocity, shear rate, basal stress) is stored for each (x,y) point in the computational grid. This greatly boost the performance of the code. In this respect, the apex "3D" only refers to the capability of the code to read and solve 3D topographies. In HYBIRD, on the other hand, there is no preferential direction and the code is solved in an equally-spaced 3D grid. Local values for velocity, pressure and shear rate are obtained for each fluid point in (x,y,z). This requires a larger allocation of resources, and much longer computational times. However, the model requires no assumption on the shape of the velocity profile, and allows to directly implement rheological laws, returning a complete 3D velocity filed.

Three different study cases are studies with RASH^{3D}. HYBIRD, which is still under development, has been used to tentatively reproduce one of the cases. After a short presentation of the two models, the results for each case are presented.

2 Theoretical aspects of RASH[3D]

The numerical code RASH[3D] is based on a one-phase continuum mechanics approach, and on depth-averaged St. Venant equations. The real heterogeneous mass is replaced with an incompressible equivalent fluid, whose behaviour is described by the depth-averaged balance equations of mass and momentum:

$$\begin{cases} \dfrac{\partial h}{\partial t} + \dfrac{\partial (v_x h)}{\partial x} + \dfrac{\partial (v_y h)}{\partial y} = E_t \\ h\left(\dfrac{\partial v_x}{\partial t} + v_x \dfrac{\partial v_x}{\partial x} + v_y \dfrac{\partial v_x}{\partial y}\right) = \dfrac{1}{2}\dfrac{\partial (K_x g_z h^2)}{\partial x} = \dfrac{1}{\rho}\tau_{zx} + g_x h - v_x E_t \\ h\left(\dfrac{\partial v_y}{\partial t} + v_x \dfrac{\partial v_y}{\partial x} + v_y \dfrac{\partial v_y}{\partial x}\right) = \dfrac{1}{2}\dfrac{\partial (K_y g_z h^2)}{\partial y} = \dfrac{1}{\rho}\tau_{zy} + g_y h - v_y E_t \end{cases} \quad (1)$$

where:

- v_x, v_y denote the depth-averaged flow velocities in the x and y directions (z is normal to the topography);
- h is the fluid depth;
- τ_{zx}, τ_{zy} are the shear resistance stresses;
- E_t is the time rate of bed erosion or "erosion rate", that is, the rate at which the path material is added to the moving mass;
- K_x, K_y are the earth pressure coefficients, that is, the ratio of the longitudinal stresses to the normal stress;
- ρ is the mass density
- g_x, g_y, g_z are the projections of the gravity vector in the x-, y-, z- directions, respectively.

The governing equations (1) are solved in RASH[3D] using an Eulerian framework, on a triangular finite element mesh, through a kinetic scheme that is based on a finite volume (Mangeney-Castelnau et al. 2003).

2.1 Rheological kernel

The rheology of the material is modelled by a single term, which describes the basal shear stress that develops at the interface between the moving mass and the sliding surface. A geographic information system (GIS) integrated function makes it possible to change the type of rheology and/or the rheological parameter values along the run-out path to allow changes to be made to the flow characteristics during flow propagation (Pirulli et al., 2017).

The following relationships are implemented in RASH[3D]:

(a) Frictional rheology, the resisting shear forces at the base of the flowing mass are assumed to depend on the normal stress, but not on velocity

$$\tau_{zi} = -(\rho g h \tan\varphi)\frac{v_i}{\|\boldsymbol{v}\|} \quad (2)$$

where φ is the dynamic basal friction angle;

(b) Turbulent rheology, which is characterized by intense mixing, at relatively high inertial to viscous stress ratios. The turbulent basal shear resistance is proportional to the square of the depth-averaged flow velocity, and it can be calculated using the Manning equation:

$$\tau_{zi} = -\left(\frac{\rho g n^2 h v_i^2}{h^{1/3}}\right)\frac{v_i}{\|\boldsymbol{v}\|} \quad (3)$$

where n is the Manning roughness coefficient, and the subscript $i = x, y$, respectively.
A commonly used alternative to equation (2) is the Chézy equation:

$$\tau_{zi} = -\left(\frac{\rho g v_i^2}{C^2}\right)\frac{v_i}{\|\boldsymbol{v}\|} \quad (4)$$

where C is the Chézy coefficient, which is related to the Manning coefficient (n) by $C = h^{1/6}/n$.
One disadvantage of this approach is that it cannot reproduce the cessation of motion on gently sloping surfaces. Nevertheless, Costa (1997) and Jin and Fread (1999) showed that the flow depth and the velocity of a channelized flowing mass can be simulated reasonably well after calibration with Manning or Chézy coefficients;

(c) Voellmy rheology, where the turbulent rheology disadvantage can be overcome by adding a frictional term in the rheological formulation that describes the stopping of the flow on a sloping surface (e.g. Hungr and McDougall 2009, Naef et al. 2006, Rickenmann et al. 2006). It results

$$\tau_{zi} = -\left(\rho g h \tan\varphi + \frac{\rho g v_i^2}{C^2}\right)\frac{v_i}{\|\boldsymbol{v}\|} \tag{5}$$

which consists of a turbulent term, $\xi = C^2$ that accounts for velocity-dependent friction losses, and a Coulomb or basal friction term, ($\tan\varphi$), which is used to describe the stopping mechanism, where the basal friction angle φ is generally only a fraction of the Coulomb angle;

(d) Bingham rheology, which combines plastic and viscous behaviors. A so-called Bingham fluid behaves like a rigid material below a given threshold yield strength, but like a viscous material above this threshold. The basal shear resistance can be determined by solving the following cubic equation:

$$\tau_{zi}^3 + 3\left(\frac{\tau_0}{2} + \frac{\nu_B v_i}{h}\right)\tau_{zi}^2 - \frac{\tau_0^3}{2} = 0 \tag{6}$$

where τ_0 is the Bingham yield stress and ν_0 is the Bingham viscosity. The third-order polynomial has been solved and implemented in RASH^{3D} using the polynomial economization technique proposed by Pastor et al. (2004);

(e) Quadratic rheology, in which the shear resistance stress is provided by the following expression:

$$\tau_{zi} = -\left(\tau_0 + \frac{k\nu_0}{8h}|v_i| + \rho g\frac{n_{td}^2 v_i^2}{h^{\frac{1}{3}}}\right)\frac{v_i}{\|\boldsymbol{v}\|} \tag{7}$$

where n_{td} is the equivalent Manning coefficient for turbulent and dispersive shear stress components and k is the flow resistance parameter (O'Brien et al. 1993).

2.2 Erosion rate formula

In consideration of the fact that 1) numerical models are nowadays still empirically based and cannot describe the complex internal mechanics of a flowing mass, and 2) a lack of information of entrainment process complexity and dynamics exists, if a concept can be devised to define how much mass is available to be entrained, simple entrainment models are adequate to describe the overall mass of an event.
This is why, after a review of existing approaches to entrainment, the simple law proposed by McDougall & Hungr (2005) has been selected for implementation in RASH^{3D} (Pirulli and Pastor, 2012), because it presents a very good combination of simplicity and accuracy:

$$E_t = E_s h\boldsymbol{v} \tag{8}$$

Assuming that the total volume V_f mobilized by a landslide is given by the sum of the released volume V_0 (accounting for expansion due to fragmentation of the initial failure) and the entrained volume V_e, E_s can be obtained directly from the initial (V_0) and final ($V_f = V_0 + V_e$) volumes of the material and the length of the erosion path (l) as

$$E_s = \ln(V_f/V_0)/l \tag{9}$$

In RASH^{3D}, areas with erodible material and maximum erosion depths or maximum erosion volumes have to be defined by user. Entrainment occurs when moving mass crosses the above mentioned areas. The erosion can have finite or infinite values that means a finite value of maximum erosion depth or volume or an infinite value of erosion depth or volume, respectively.

3 Theoretical aspects of HYBIRD

HYBIRD is a code originally conceived as a combination of the Discrete Element Method (DEM) and LBM (Leonardi et al., 2014; Leonardi et al., 2015). The development eventually aims at a multi-phase description of the mass, with the largest grains resolved with DEM, and the remaining mass with LBM. This work sees the first application of the code at the full topographical scale. Therefore, to limit the number of unknowns, only the LBM part of the code is tested.

HYBIRD utilizes concepts from the kinetic theory, and discretizes an Eulerian probability density function (pdf) $f(\boldsymbol{x}, \boldsymbol{c}, t)$, which indicates the probability of finding a fluid particle with microscopic velocity $\boldsymbol{c}$ at position $\boldsymbol{x}$ and time t. In addition to the usual discretization in the time- and space domains, also the velocity space is discretized by selecting only a finite set of allowed microscopic velocities $\boldsymbol{c}_i$. Thus, the discretized for of the pdf reads $f_i(\boldsymbol{x}, t) = f(\boldsymbol{x}, \boldsymbol{c}_i, t)$. The standard macroscopic velocity and density fields are then reconstructed by simple summation at every node:

$$\rho(\boldsymbol{x}, t) = \sum_i f_i(\boldsymbol{x}, t)\,; \quad \boldsymbol{v}(\boldsymbol{x}, t) = \sum_i f_i(\boldsymbol{x}, t)\boldsymbol{c}_i\,/\rho(\boldsymbol{x}, t) \tag{10}$$

The evolution of the pdf is controlled by the Boltzmann equation:

$$\frac{df}{dt} = \Omega_{coll} \tag{11}$$

where Ω_{coll} is the collision operator, implementing the effect of viscous dissipation. The time discretization is explicit. For the full formulation and the theoretical background, please refer to Chen & Doolen (1998). The algorithm also features a free surface tracker based on a volume-of-fluid approach. However, no erosion model is currently implemented, and the flowing mass conserves exactly. Note that the shear rate tensor $\dot{\gamma}_{ij}$ can be computed locally directly from the pdf, and thus the calculus of no velocity gradient is required (Leonardi et al., 2014).

3.1 Rheological models

As there is no depth-integration procedure, stresses are applied everywhere on the domain, and are controlled by the rheological model, which can be chosen among the following:

a) Bingham rheology. Linear shear-thinning behavior, analogous to the one implemented in RASH^{3D}

$$\tau_{ij} = \frac{\tau_0 \dot{\gamma}_{ij}}{|\dot{\gamma}|} + \nu_0 \dot{\gamma}_{ij} \tag{12}$$

b) Turbulent rheology. A turbulent viscosity is computed according to the Smagorinsky-Lily model (Leonardi et al. 2011), with a constant subgrid turbulence constant $C_s = 0.16$.

$$\tau_{ij} = \nu_0 \dot{\gamma}_{ij} + \rho \Delta x^2 C_S^2 |\dot{\boldsymbol{\gamma}}| \dot{\gamma}_{ij} \tag{13}$$

c) Frictional rheology with rate-dependent friction coefficient

$$\tau_{ij} = \frac{\mu(I) p \dot{\gamma}_{ij}}{|\dot{\gamma}|}; \tag{14}$$

Here the friction coefficient μ is chosen to be a function of the Inertial number, a dimensionless quantity locally defined as $I = d|\dot{\boldsymbol{\gamma}}|/\sqrt{p/\rho}$, with d the grain diameter (Jop et al., 2006). The relationship $\mu(I)$ contains the three empirical constants $\Delta\mu$, μ_0, and I_0. Note that if $\Delta\mu = 0$ the model reduces to a simpler frictional model with constant coefficient.

d) Voellmy rheology. It combines frictional properties and turbulent dissipation:

$$\tau_{ij} = \frac{\tan\varphi p\dot{\gamma}_{ij}}{|\dot{\boldsymbol{\gamma}}|} + \rho d^2|\dot{\boldsymbol{\gamma}}|\dot{\gamma}_{ij} \tag{15}$$

The turbulent dissipation is mesh-independent and is controlled by a Bagnold-like collisional length scale, which can be assumed to be the grain diameter d.

One of the main difficulty of working outside the depth-averaged framework is the calibration of the rheological parameters. As those are usually back-calculated, and are not directly obtained from the physical properties of the material, there is no guarantee that the same parameters will yield similar results when transferred from RASH^{3D} to HYBIRD.

4 BENCHMARKING

This section presents and discusses the results obtained with RASH^{3D} in the numerical analysis of two cases of back-analysis: the Yu Tung debris flow (Hong Kong) and the Johnsons Landing debris avalanche (Canada); and one case of forward-analysis at an historical hillside catchment (Kun Yam Shan) in Hong Kong. The Yu Tung debris flow is also back-calculated using HYBIRD.

4.1 Benchmark C1 – 2008 Yu Tung Road debris flow, Hong Kong

The Yu Tung debris flow was recorded in June 2008, when a mass of about $2350\ \mathrm{m}^3$ detached from a hillslope and invaded a nearby road. There is rich documentation about the event (AECOM, 2012), with velocity estimations at various locations, as shown in Fig. 1.



Figure 1: Picture of the Yu Tung debris flow. The five sections indicate chainages (CH) where velocity estimates are available: A: CH100; B: CH413; C: CH439; D: CH462; E: CH477.

Accordingly to previously calibrated case histories in Hong Kong and to specific analyses carried out for the 2008 Yu Tung Road debris flow by Tattersall et al. (2009) (Table 1), the RASH^{3D} numerical back analyses were carried out using either a Frictional (Case1) or a Voellmy rheology (Case2) in the source area combined with a Voellmy rheology along the runout channel for both the Case1 and Case2. In particular, the change of rheology or values of rheological parameters between the source and the runout channel was necessary to simulate

observed deposition of about 300 m^3 of debris within the landslide source area. Furthermore, accordingly to on-site estimate, erosion rates was considered between CH65 and CH340 to allow the active volume to increase to a maximum of about 3.345 m^3 by CH340. A space discretization $\Delta x = \Delta y = 2$ m is adopted.

Table 1: Yu Tung debris flow. Calibrated parameters from Tatterstal et al. (2009)

	Source		Channel		
Model	Debriflo /2d-DMM	DAN3D	Debriflo / 2d-DMM	DAN3D	Case
Rheology	Voellmy	Frictional	Voellmy	Voellmy	
Parameters	$\varphi = 23°, \xi = 845$ m/s^2	$\varphi = 28°$	$\varphi = 11.3°, \xi = 500$ m/s^2	$\varphi = 8.5°, \xi = 750$ m/s^2	1
			$\varphi = 7.5°, \xi = 750$ m/s^2		2

Starting from the Tatterstal et al. set of rheological values, RASH^{3D} results are calibrated by trial-and-error to reproduce the flow dynamics in terms of on-site estimated velocities at the above mentioned chainages and capability of the simulated landslide debris to reach the road. The best fit rheological parameters for RASH^{3D} are resumed in Table 2. It can be observed that the calibrated values are very close to those obtained by Tatterstal et al. (2009) with Debriflo, 2d-DMM and DAN3D (Table 1).

Table 2: Yu Tung debris flow. Calibrated parameters for RASH^{3D}

	Source		Channel
Rheology	Voellmy	Frictional	Voellmy
Case 1		$\varphi = 25°$	$\varphi = 8.5°, \xi = 750$ m/s^2
Case 2	$\varphi = 23°, \xi = 845$ m/s^2		$\varphi = 8.5°, \xi = 750$ m/s^2

The Yu Tung debris flow is also back-analyzed using HYBIRD. In this case, the rheological parameters used in precedent works and for RASH^{3D} cannot be directly tested. However, some principles can be transferred, in particular the use of a Voellmy rheology, with a low angle of friction. The space discretization is $\Delta x = \Delta y = \Delta z = 0.4$ m. In HYBIRD different rheologies were tested, as shown in Table 3. In each case, the same rheology has been used consistently over the whole domain. Shear resistance is active in any direction, and at every location inside the 3D mass. Probably due to this reasons, lower friction angles should be used to obtain results consistent with depth-averaged models and with the field data.

Table 3: Yu Tung debris flow. Calibrated parameters for HYBIRD

	Dissipation source			
	Frictional	Collisional	Plastic	Viscous
Case 1: Voellmy	$\varphi = 6°$	$d = 0.005$ m	/	/
Case 2: Voellmy	$\varphi = 4°$	$d = 0.02$ m	/	/
Case 3: Voellmy	$\varphi = 1.5°$	$d = 0.005$ m	/	/
Case 4: Bingham	/	/	$\tau_0 = 500$ Pa	$\nu_0 = 20$ Pa s
Case 5: Turbulent	/	/	/	$\nu_0 = 50$ Pa s

The flow velocity along the talweg is shown in Figure 2, with results of the two cases studied with RASH^{3D} (Case 1 and Case 2) and the best results obtained with HYBIRD (Case 3). The available field data is also reported with yellow markers. A rather good fit of velocities is observed for both models. The results evidence that, albeit substantial differences in the approach, RASH^{3D} and HYBIRD give approximately the same values of flow velocities overall, and especially at chainages where the on-site flow velocity was estimated based on flow super-elevation. Note that for HYBIRD surface velocities are also available (i.e. not depth averaged). These are reported in the graph.

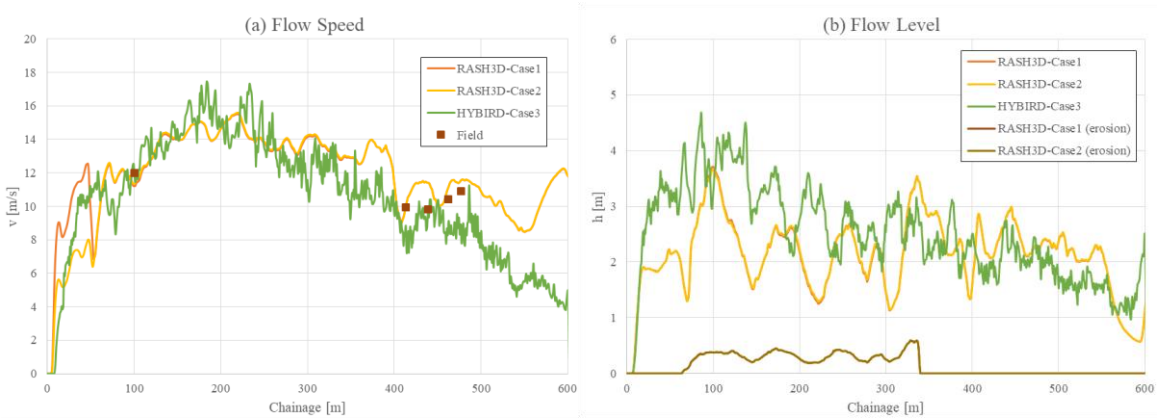


Figure 2: Yu Tung debris flow. (a) Comparison between RASH^{3D} and HYBIRD in terms of maximum flow speed (depth-averaged) and estimated velocities of the Yu Tung Debris Flow (brown squares). Please see Figure 1 and 2a for the approximate locations of velocity records. (b) Comparison between RASH^{3D} and HYBIRD in terms of simulated flow depth along the runout path. For RASH^{3D}, also erosion depth are available (same for the two cases).

As for the landslide debris spatial distribution during the runout process up to the final deposition, it is observed that for both models the whole mass reaches the road, see Figure 3. For RASH^{3D}, since Case 1 better fits the deposition of debris in the source area (Figure 3 left column), its representation in terms of flow process is given in the figure.

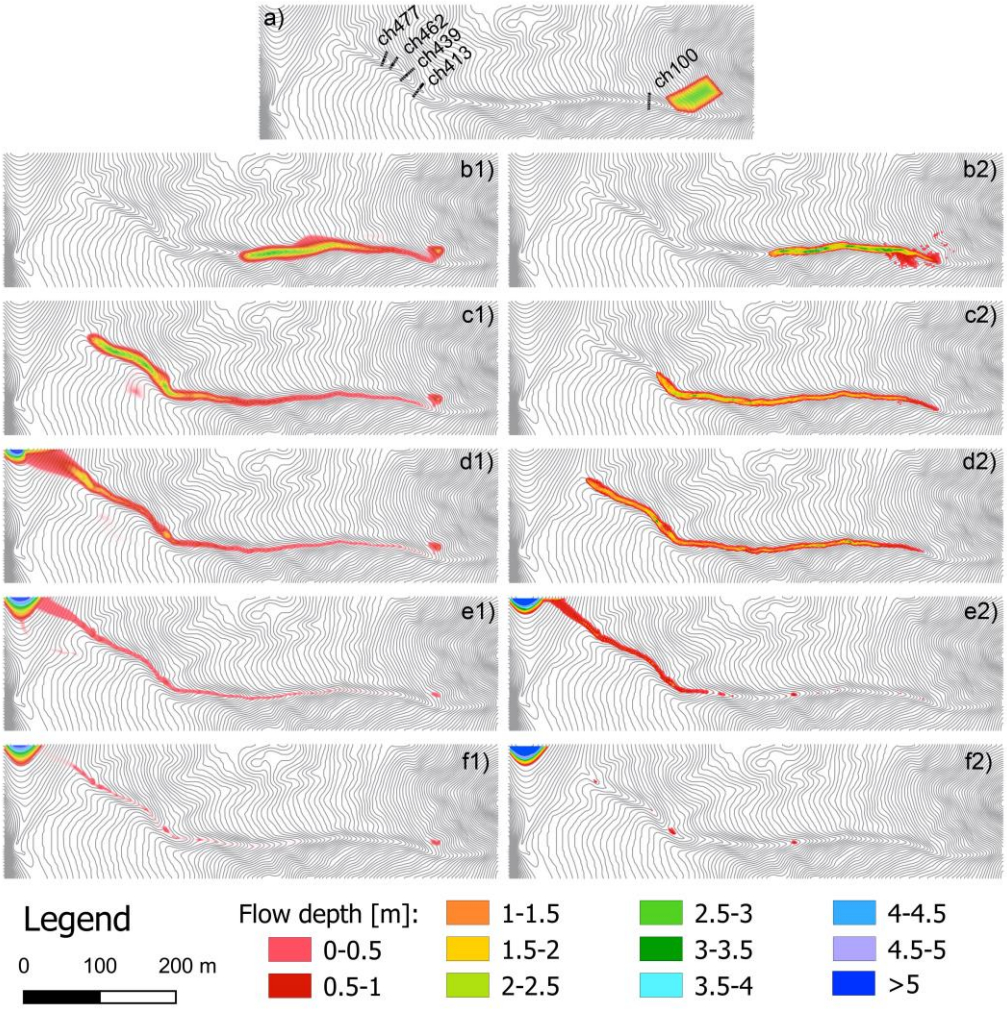


Figure 3: Yu Tung debris flow. Flow runout path, with flow-depth contours at different times: (a) 0 s, (b) 20 s, (c) 40 s, (d) 60 s, (e) 100 s, (f) 300 s. The left column shows the results obtained with RASH^{3D}, the right column those obtained with HYBIRD.

4.2 Benchmark C2 – Johnsons Landing debris avalanche, Canada

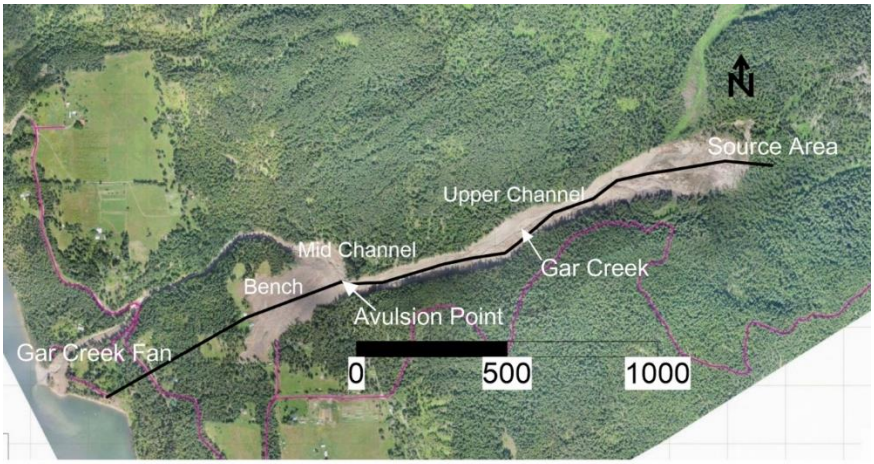


Figure 4: Aerial view of the area interested by the Johnsons debris avalanche. Copyright © Province of British Columbia.

The Johnsons (Canada) debris avalanche occurred in 2012, when about $320000\ \mathrm{m}^3$ of unstable material flowed inside the Gar creek, overtopping its left bank at a sharp bend, and finally depositing both inside the main channel and on a lateral bench. While the area was already known for its activity, the flow path was unusual. Debris invaded a settled area, with four casualties (Nicol et al., 2013). An estimation of the mass deposited on the bench, middle- and upper channel is also available, respectively $169000\ \mathrm{m}^3$ $55000\ \mathrm{m}^3$, and $40000\ \mathrm{m}^3$ (Nicol et al., 2013).

The RASH^{3D} back analysis of the Johnsons landing debris avalanche is carried out with the Voellmy and the Quadratic rheologies, and results are compared. A calibration of the Voellmy rheology parameters gave good back analysis results using a frictional coefficient $\tan\phi = 0.2$ and a turbulence coefficient $\xi = 800\ \mathrm{m/s^2}$ (Table 4 Case 3V). While, in case of Quadratic rheology the combination, 1.2 kPa, 40 Pa s and $0.03\ \mathrm{s\ m^{-1/3}}$ for Bingham yield stress, Bingham viscosity and equivalent Manning coefficient, respectively, was obtained (Table 4 Case 4Q).

Table 4: Johnsons Landing debris avalanche. Parametric analyses carried out with the two adopted rheologies in RASH^{3D}.

Voellmy			Quadratic			
Case	$\xi\ [\mathrm{m/s^2}]$	$\tan\varphi$ [°]	Case	τ_0 [kPa]	η [kPa s]	$n_{td}\ [\mathrm{s\ m^{-1/3}}]$
1V	500	0.15	1Q	1.2	0.01	0.1
2V	500	0.20	2Q	1.2	0.04	0.1
3V	800	0.20	3Q	1.2	0.04	0.03
4V	500	0.25	4Q	8.0	0.04	0.03
			5Q	6.0	0.04	0.03
			6Q	8.0	0.03	0.03

A comparison between on-site estimate and numerical simulations of debris volume deposited along the runout path (Table 5Table 5: Johnsons Landing debris avalanche. Comparison between estimated and computed volumes (RASH^{3D}) as deposited along the runout path.) evidenced that the Voellmy combination of parameters rather approximated the volumes that deposited in the mid-channel but underestimated those deposited on the bench. Similarly, too much debris reached the channel downstream of the bend (lower channel) and too little material deposited in the upper channel (Figure 5a). As to the Quadratic rheology, the same observations can be made in terms of volume deposited on the bench and on the mid-channel, while volumes deposited along the upper channel resulted more realistic (Figure 5b).

Table 5: Johnsons Landing debris avalanche. Comparison between estimated and computed volumes (RASH^{3D}) as deposited along the runout path.

	Upper channel [m^3]	Mid channel [m^3]	Bench [m^3]
Estimate	140000	55000	169000
Case 3V	2541	25444	81091
Case 4Q	98885	37348	81693

However, Marinelli et al. (2015) and Nicol et al. (2013) observed that a channel obstruction existed downstream of the 70° bend due to an accumulation of timber, stripped from the upper slopes of the gully and entrained at the flow front, getting jammed due to a narrowing of the channel.

This obstruction was assumed by those Authors and it has been implemented in a second set of numerical analyses carried out with RASH^{3D}. The new results obtained with the Voellmy (Case 3V) and the Quadratic (Case 4Q) are reported in Figure 5c and Figure 5d, respectively. In both the cases the channel obstruction modifies the volume deposited in the mid-channel, while that on the bench and in the upper channel remains rather unchanged.

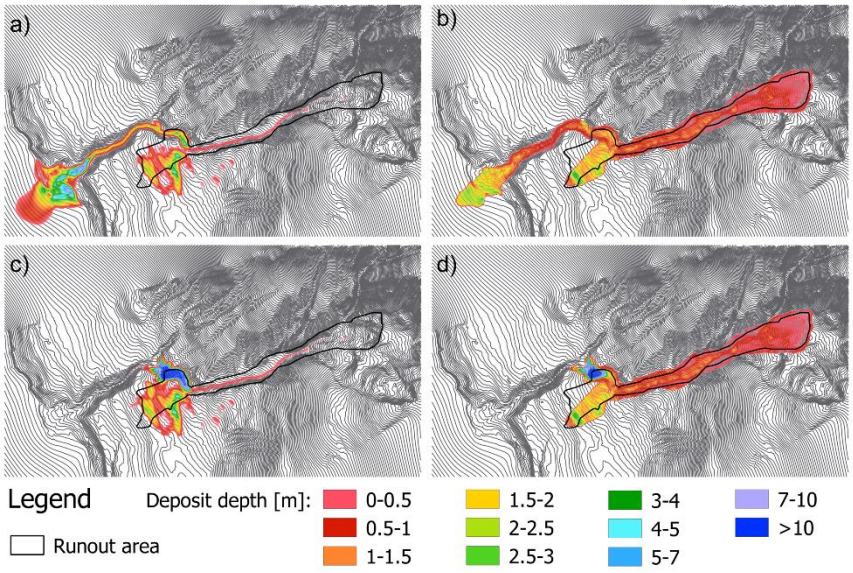


Figure 5: Johnsons Landing debris avalanche. Comparison between on-site surveyed runout area and RASH3D results without channel obstruction: (a) Voellmy rheology - Case 3V; (b) Quadratic rheology – Case 4Q; and with channel obstruction: (c) Voellmy rheology - Case 3V; (d) Quadratic rheology – Case 4Q.

4.3 Benchmark D1 – A historical hillside catchment in Hong Kong

This study case analyses the Tates's Cairn area in Hong Kong, where an historical debris flow was already recorded in 2005. The historical case has already been analysed in the past using RASH^{3D} by (Pirulli & Scavia, 2007). A second potentially unstable mass, located in nearby Kun Yam Shan**,** is the subject of the following study.

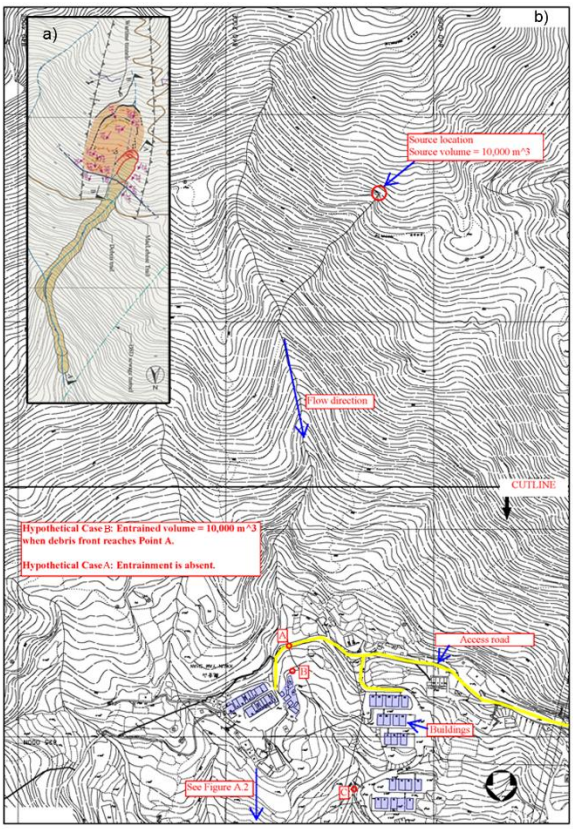


Figure 6: Kun Yam Shan. (a) Plan view of the 2008 debris flow (brown area) and extent of distressed hillside (orange area); (b) plan view of flow direction with indication of observation points A, B and C position.

Based on previously calibrated case histories in Hong Kong and on indications given by the Technical Guidance Note (TGN 29) of the Hong Kong Geotechnical Engineering Office, a Voellmy rheology was assumed in the carried out analyses. Furthermore, for safety reasons, both the suggested sets of Voellmy parameters, $\varphi = 8°$, $\xi = 500\ \mathrm{m/s^2}$ (Case 1) and $\varphi = 11°$, $\xi = 500\ \mathrm{m/s^2}$ (Case 2), to be used for channelized debris flow catchments that are deemed to be prone to watery debris and that are not associated with this adverse site settings, respectively, were tested (TGN 29).

Even if these sets of parameters are suggested for use in the computer programs 2d-DMM, DAN and 3d-DMM (TGN 29), their use in RASH^{3D} was justified by the fact that RASH^{3D} adopts an analytical approach that is close to that of the above mentioned codes and it has been found to produce generally similar results in terms of runout distance, velocity and thickness profile of debris in the back analyses of some landslides in Hong Kong and elsewhere (e.g. Sauthier et al., 2010, 2015; McDougall et al., 2008).

Both Case 1 and Case 2 analyses are carried out with RASH^{3D} assuming (i) entrainment does not occur and (ii) entrainment occurs and the entrainment volume is 10,000 m^3 when the debris front reaches the road (Figure 6, point A). The carried out analyses, with the adopted rheological values, are summarized in Table 6.

Table 6: Kun Yam Shan. Sets of rheological parameters for the analysis carried out with RASH^{3D}.

Case	φ [°]	ξ [m/s^2]	E_s [m^{-1}]
1A	8	500	-
1B	8	500	0.0025
2A	11	500	-
2B	11	500	0.0025

Simulation results in terms of velocity and debris thickness hydrographs at points A, B and C (Figure 6) are illustrated in Figure 7. For all the observation points, it results that a maximum velocity of about 8 m/s, and a

minimum debris thickness of about $1 - 1.5$ m, are reached with the analysis of Case 1A. A minimum velocity of about $2 - 4$ m/s, and a maximum debris thickness of about $2 - 3$ m, are obtained with the analysis of Case 2B.

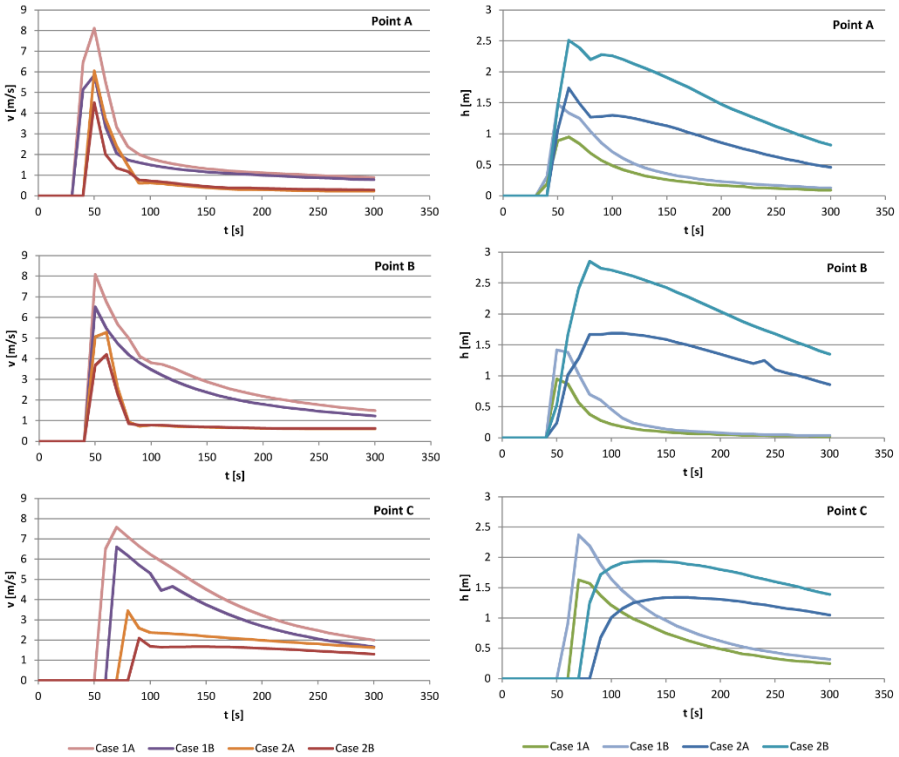


Figure 7: Kun Yam Shan. Velocity and debris thickness hydrographs obtained with RASH^{3D} at points A, B and C (see Figure 6) for all Cases.

The time history of average velocity of the debris along the flow path is resumed for the Case 1B in Figure 8 (a) for the most significant time steps; the same analysis is made in terms of time history of the debris active volume (i.e. source volume + entrained volume) along the flow path in Figure 8 (b) and (c), respectively. Case 1B is selected since it is the case with active entrainment in which the flowing mass reaches the highest velocity. This is spite of the flow depth not reaching the maximum at the above mentioned observation points (the faster the mass, the thinner it will be).

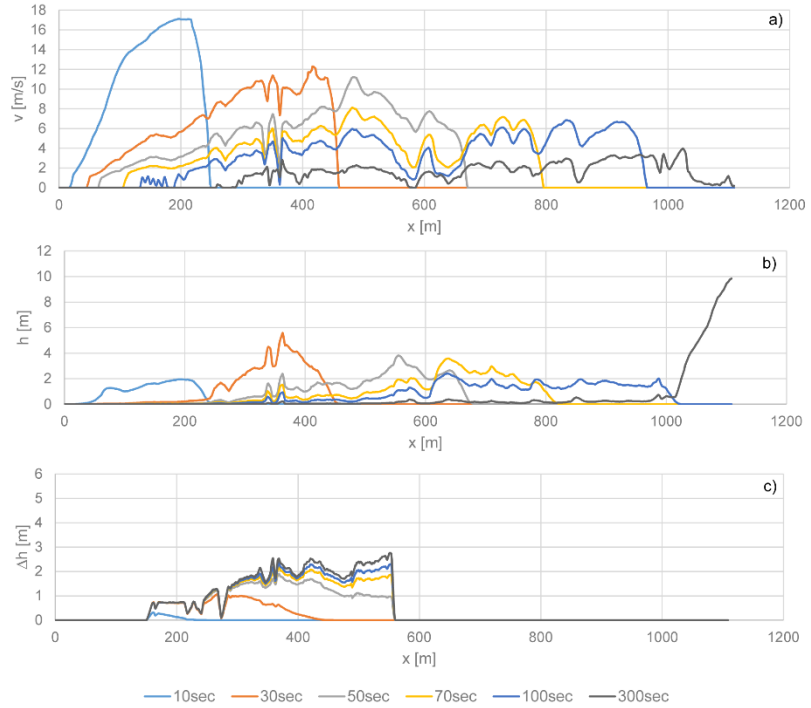


Figure 8: Kun Yam Shan, Case 1B (RASH^{3D}). (a) Time history of average velocity of landslide debris along the flow path; (b,c) Time history of active volume (i.e. source volume + entrained volume) of landslide debris along the flow path.

The profiles of landslide debris throughout the flow process are also reported in Figure 9. It results that with the adopted rheology and rheological parameters, the landslide debris reaches the road and the buildings downstream of the road. As already shown in Figure 7, the same considerations can be made for all carried out analyses (Table 6Table 6: Kun Yam Shan. Sets of rheological parameters for the analysis carried out with RASH^{3D}.).

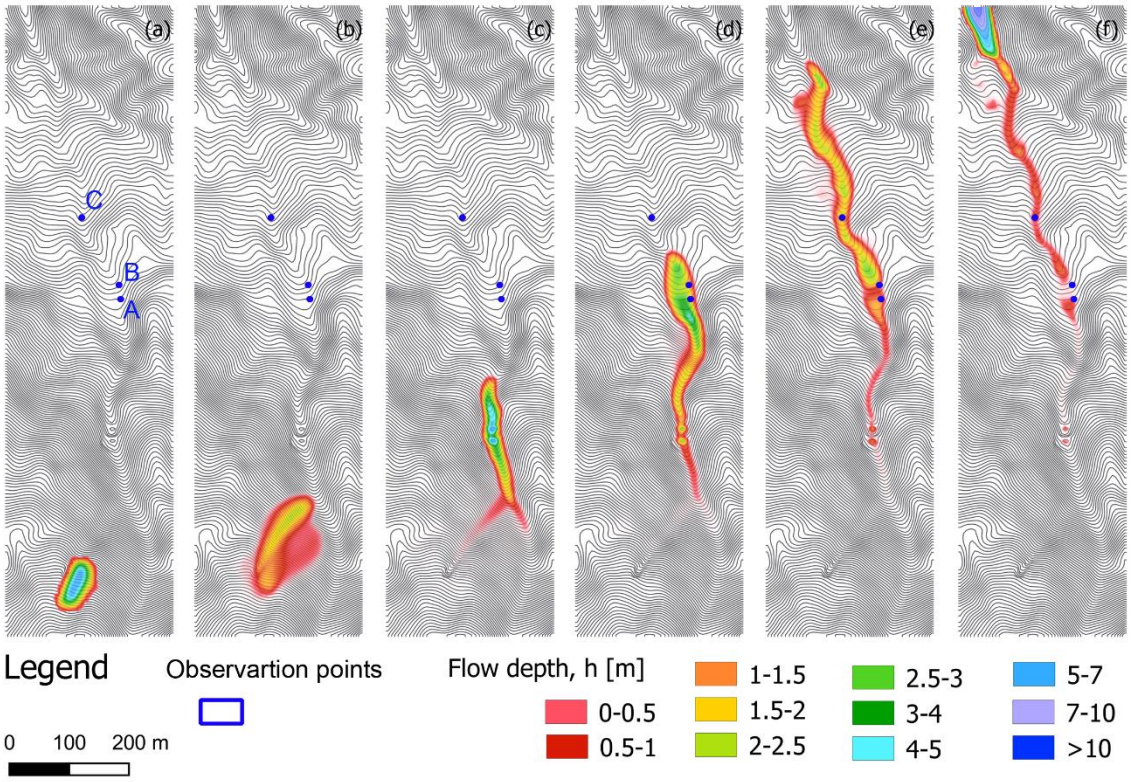


Figure 9: Kun Yam Shan, Case 1B (RASH^{3D}). Profiles of flow depth throughout the flow process.

5 CONCLUSIONS

In this work, we presented the results obtained for three study cases. The Yu Tung debris flow (Hong Kong) has been analyzed with RASH^{3D}, a depth-averaged model, and also with HYBIRD, a full-3D code based on LBM. Two additional cases have been studied only with RASH^{3D}: the Johnsons debris flow (Canada), and a potential instable area in Kun Yam Shan (Hong Kong). For all cases, a good comparison with the field data has been obtained. The cross comparison carried out for Yu Tung represents one of the first attempt at moving beyond the depth-averaging paradigm. Once validated, HYBIRD can also be used to simulate structural countermeasures of arbitrary shape. Future studies will focus on this aspect.

ACKNOWLEDGEMENTS

Computational resources were provided by HPC@POLITO, a project of Academic Computing within the Department of Control and Computer Engineering at Politecnico di Torino (http://www.hpc.polito.it)

REFERENCES

AECOM. 2012. Detailed Study of the 7 June 2008 landslides on the hillside above Yu Tung Road, Tung Chung. GEO Report No. 271, 124 p.

Chen, S., & Doolen, G. D. 1998. Lattice Boltzmann Method for Fluid Flows. *Annual Review of Fluid Mechanics*, 30, 329–364.

Costa, J.E. 1997. Hydraulic modeling for Lahar hazards at Cascades Volcanoes. *Environmental & Engineering Geoscience* III(1): 21–30.

Froude, M. J., & Petley, D. N. 2018. Global fatal landslide occurrence from 2004 to 2016. *Natural Hazards and Earth System Sciences*, 18(8), 2161–2181.

Hungr, O. & McDougall, S. 2009. Two numerical models for landslide dynamic analysis. *Computers & Geosciences* 35(5): 978-992.

Jin, M. & Fread, D.L. 1999. 1D modeling of mud/debris unsteady flows. *J. Hydrol. Eng.* 125(8): 827–834.

Jop, P., Forterre, Y., & Pouliquen, O. 2006. A constitutive law for dense granular flows. *Nature*, 441(7094), 727–30.

Leonardi, C. R., Owen, D. R. J., & Feng, Y. T. 2011. Numerical rheometry of bulk materials using a power law fluid and the lattice Boltzmann method. *Journal of Non-Newtonian Fluid Mechanics*, *166*(12–13), 628–638.

Leonardi, A., Wittel, F. K., Mendoza, M., & Herrmann, H. J. 2014. Coupled DEM-LBM method for the free-surface simulation of heterogeneous suspensions. *Computational Particle Mechanics*, 1, 3–13.

Leonardi, A., Cabrera, M., Wittel, F. K., Kaitna, R., Mendoza, M., Wu, W., & Herrmann, H. J. 2015. Granular-front formation in free-surface flow of concentrated suspensions. *Physical Review E - Statistical, Nonlinear, and Soft Matter Physics*, 92(5), 052204.

Leonardi, A., Wittel, F. K., Mendoza, M., Vetter, R., & Herrmann, H. J. 2016. Particle-Fluid-Structure Interaction for Debris Flow Impact on Flexible Barriers. *Computer-Aided Civil and Infrastructure Engineering*, 31(5), 323–333.

Mangeney-Castelnau, A., Vilotte, J.P., Bristeau, M.O., PerthameE, B., Bouchut, F., Simeoni, C., Yerneni, S., 2003. Numerical modelling of avalanche based on saint Venant equations using a kinetic scheme. *Journal of Geophysical Research*, 108(B11).

Marinelli, G., Aaron, J., Borgatti, L., Jordan, P., & Hungr, O. 2015. Back Analysis of Johnsons Landing 2012 Landslide Using Two Dynamic Analysis Models. In G. Lollino, D. Giordan, G. B. Crosta, J. Corominas, R. Azzam, J. Wasowski, & N. Sciarra (Eds.), *Engineering Geology for Society and Territory - Volume 2: Landslide Processes*, 1267–1270, Springer International Publishing.

McDougall, S., Pirulli, M., Hungr, O. & Scavia, C. 2008. Advances in landslide continuum dynamic modelling. Special Lecture. In Z. Chen et al. (eds), *Landslides and Engineered Slopes: Procs. 10th International Symposium on Landslides and Engineered Slopes*, Xi'an (China), 2008, Taylor & Francis Group, London, Vol. 1, 145-157.

McDougall, S. & Hungr, O. 2005. Dynamic modelling of entrainment in rapid landslides. *Can. Geotech. J.* 42(5): 1437–1448.

Naef, D., Rickenmann, D., Rutschmann, P. & McArdell, B. 2006. Comparison of flow resistance relations for debris flows using a one-dimensional finite element simulation model. *Natural Hazards and Earth System Science* 6: 155-165.

Nicol, D., Jordan, P., Boyer, D., & Yonin, D. 2013. Regional District of Central Kootenay (RDCK) Johnsons Landing Landslide Hazard and Risk Assessment. Regional District of Central Kootenay (RDCK) Johnsons.

O'Brien, J.S., Julien, P.Y. & Fullerton, W.T. 1993. Two-dimensional water flood and mud flow simulation. *Journal of Hydraulic Engineering* 119(2): 244–261.

Pastor, M., Quecedo, M., Gonzalez, E., Herreros, M.I., Fernandez Merodo, J.A. & Mira, P. 2004. Simple approximation to bottom friction for Bingham fluid depth integrated models. *Journal of Hydraulic Engineering* 130(2): 149-155.

Pirulli, M. 2005. Numerical modelling of landslide runout, a continuum mechanics approach. Dissertation, Politecnico di Torino, Torino, Italy.

Pirulli, M., & Scavia, C. 2007. A set of benchmarking tests to assess the performance of a continuum mechanics depth-averaged model. In K. Ho & V. Li (Eds.), *The 2007 International Forum on Landslide Disaster Management* (pp. 1015–1042). Hong Kong.

Pirulli, M., Bristeau, M.O., Mangeney, A. & Scavia, C. 2007. The effect of the earth pressure coefficients on the runout of granular material. Environmental Modelling & Software, 22(10), 1437-1454.

Pirulli M. & Pastor M. 2012. Numerical study on the entrainment of bed material into rapid landslides. *Geotechnique*, 62(11), 959-972.

Pirulli, M., Barbero, M., Marchelli, M. & Scavia, C. 2017. The failure of the Stava Valley tailings dams (Northern Italy): numerical analysis of the flow dynamics and rheological properties. *Geoenvironmental Disasters*, 4(3), 1-15.

Rickenmann, D., Laigle, D., McArdell, B. & Hubl, J. 2006. Comparison of 2D debris-flow simulation models with field events. *Computational Geosciences* 10: 241-264.

Sauthier, C., Pirulli, M., Pisani, G., Scavia, C. & Labiouse, V. 2015. Numerical modelling of gravel unconstrained flow experiments with the DAN3D and RASH3D codes, *Computers & Geosciences*, 85, 81-90.

Sauthier, C., Labiouse, V., Pirulli, M. & Scavia, C. 2010. Numerical simulation of gravel unconstrained flow experiments: a comparison between DAN-3D and RASH-3D codes. In J. Zhao et al. (eds), *Rock Mechanics in Civil and Environmental Engineering: Procs. of the European Rock Mechanics Symposium (EUROCK 2010)*, 2010, Taylor & Francis Group, London, Vol. 2, 571-574.

Tattersall, J.W., Devonald, D.M. & McDougall, S. 2009. Modelling of debris flows for the North Lantau Expressway and Tu Tung Road study area. In *Procs. of the HKIE Geotechnical Division 29th Annual Seminar*, The Hong Kong Institution of Engineer, Geotechnical Division, 163-169.